Research Article Vol. 56, No. 13 / May 1 2017 / Applied Optics 3879

applied optics

Alignment sensing for optical cavities using radio-frequency jitter modulation

P. Fulda,* D. Voss, C. Mueller, L. F. Ortega, G. Ciani, G. Mueller, and D. B. Tanner

University of Florida, Gainesville, Florida 32611, USA
**Corresponding author: pfulda@phys.ufl.edu*

Received 21 February 2017; accepted 27 March 2017; posted 6 April 2017 (Doc. ID 287112); published 1 May 2017

Alignment sensing is often required in precision interferometry applications such as Advanced LIGO in order to achieve the optimum performance. Currently favored sensing schemes rely on the use of two separate radio-frequency (RF) quadrant photodetectors and Gouy phase telescopes to determine the alignment of a beam relative to an optical cavity axis. In this paper, we demonstrate an alternative sensing scheme that has potential advantages over the current standard schemes. We show that by using electro-optic beam deflectors to impose RF jitter sidebands on a beam, it is possible to extract full alignment signals for two in-line optical cavities from just one single-element photodetector in reflection of each cavity.

OCIS codes: (220.1140) Alignment; (040.5160) Photodetectors; (140.3295) Laser beam characterization; (140.4780) Optical resonators; (120.3180) Interferometry; (000.2780) Gravity.

https://doi.org/10.1364/AO.56.003879

1. INTRODUCTION

The locking of lasers to optical cavities is a ubiquitous technique in the field of precision interferometry. The narrow linewidth of optical resonators makes them excellent frequency discriminators, and the Pound–Drever–Hall (PDH) method provides shot-noise-limited sensing of the offset between the laser frequency and the resonant frequency of the optical cavity [1]. A stable optical cavity also has useful mode cleaning properties, typically only resonating in a single longitudinal and spatial mode, and allows for longer storage time of photons.

The coupling of a laser into an optical cavity is optimal only when the input beam axis coincides exactly with the axis of the cavity eigenmode. In many cases, especially with cavities formed by suspended optics such as in interferometric gravitational wave detectors like Advanced LIGO [2,3], the alignment between input beam and cavity axis must be sensed interferometrically and actively controlled. Several methods are currently used to achieve this alignment sensing: dither alignment and differential wavefront sensing of the beat between carrier and radio-frequency (RF) phase modulation sidebands in reflection [4,5], or transmission [6] of the cavity with quadrant photodetectors.

We report on the theoretical description and experimental demonstration of an alternative method of alignment sensing for optical cavities. This method eliminates much of the complexity of the aforementioned differential wavefront sensing schemes, while retaining their practical benefits over simple dither alignment sensing. This alternative method makes use of electro-optic beam deflectors to produce sidebands in the first-order off-axis spatial mode (HG_{10}) separated from the carrier frequency by the higher-order mode difference frequency of the optical cavity. As we shall show, detection of the beat between these HG_{10} mode sidebands and the carrier frequency HG_{10} modes which are present when the input beam axis and cavity axis are misaligned can be made in reflection of the cavity with a single-element photodetector. In-phase and quadrature-phase (IQ) demodulation of this beat signal (as described in Section 2.C) provides at once linear error signals for both tilt and translation of the two axes in the orthogonal demodulation phases.

In Section 2 we present an analytical description of the sensing scheme for a single arbitrary Fabry–Perot cavity, and show that the results agree with a frequency-domain interferometer simulation performed using Finesse [7]. In Section 3 we describe the layout, procedure, and results of a tabletop demonstration of the alignment sensing technique on a triangular Fabry–Perot cavity. Also reported in this section is a measurement of the modulation frequency dependence of the alignment signal generated for an optical cavity, and an extension of the scheme to a second downstream cavity, in which case the requirement that the modulation frequency is equal to the higher-order mode difference frequency of the cavity is eliminated.

2. THEORY

A. Deflection Modulation

Electro-optic beam deflectors (EOBDs), such as those described in Refs. [8–10], can be used as very high bandwidth alignment actuators for beams passed through them. The effect

of actuating an EOBD at angular frequency Ω can be described by the addition of modulation sidebands around the carrier, in the first-order Hermite–Gauss (HG) mode. For now, we consider actuation in the yz plane for a beam propagating along the z axis, since by symmetry the same arguments can be applied to the actuation in the xz plane.

We describe the electric field before applying the jitter modulation as a Gaussian beam travelling in the positive z direction:

$$E(x,y,z) = E_0 \mathcal{U}_{00}(x,y,z) e^{i(\omega t - kz)} e^{-i\Psi(z)}, \tag{1}$$

where E_0 is the initial amplitude, ω is the angular frequency of the carrier light, k is the wavenumber, and $\Psi(z)$ is the Gouy phase at location z, given by

$$\Psi(z) = \arctan\left(\frac{z - z_0}{z_R}\right), \tag{2}$$

where z_0 and z_R are the beam waist location and Rayleigh range, respectively. $\mathcal{U}_{00}(x,y,z)$ is the HG_{00} mode transverse function given by

$$\mathcal{U}_{nm}(z) = (2^{n+m-1} n!m!\pi)^{-1/2} \frac{1}{w(z)} H_n\left(\frac{\sqrt{2}x}{w(z)}\right) H_m\left(\frac{\sqrt{2}y}{w(z)}\right) \times \exp\left(-\frac{ik(x^2+y^2)}{2Rc(z)} - \frac{x^2+y^2}{w(z)^2}\right), \tag{3}$$

with horizontal and vertical mode indices n and m both equal to zero. H_n and H_m are the Hermite polynomial functions, $w(z)$ is the beam radius, and $Rc(z)$ is the wavefront radius of curvature. The beam radius and wavefront radius of curvature are given as functions of z, determined by the Gaussian beam parameters w_0 (beam waist size) and z_0 (beam waist location) by

$$w(z) = w_0 + \sqrt{1 + \left(\frac{z - z_0}{z_R}\right)^2}, \tag{4}$$

$$Rc(z) = z - z_0 + \frac{z_R^2}{z - z_0}, \tag{5}$$

where z_R is the Rayleigh range, itself given by

$$z_R = \frac{\pi w_0^2}{\lambda}. \tag{6}$$

The far-field divergence angle of the beam is given by

$$\Theta = \frac{\lambda}{\pi w_0}. \tag{7}$$

In the following, we shall make use of these two approximations for describing a tilt misalignment α applied to a beam (valid for $\alpha \ll \Theta$):

$$\mathcal{U}_{00}(x,y,z) \exp\left(\frac{i2\pi\alpha y}{\lambda}\right) \approx \mathcal{U}_{00}(x,y,z) + i\frac{\alpha}{\Theta}\mathcal{U}_{01}(x,y,z), \tag{8}$$

$$\mathcal{U}_{01}(x,y,z) \exp\left(\frac{i2\pi\alpha y}{\lambda}\right) \approx \mathcal{U}_{01}(x,y,z) + i\frac{\alpha}{\Theta}(\mathcal{U}_{00}(x,y,z) + \sqrt{2}\mathcal{U}_{02}(x,y,z)). \tag{9}$$

We shall also use these two approximations for describing a translational misalignment a applied to a beam (valid for $a \ll w_0$):

$$\mathcal{U}_{00}(x,y+a,z) \approx \mathcal{U}_{00}(x,y,z) - \frac{a}{w_0}\mathcal{U}_{01}(x,y,z), \tag{10}$$

$$\mathcal{U}_{01}(x,y+a,z) \approx \mathcal{U}_{00}(x,y,z) + \frac{a}{w_0}(\mathcal{U}_{00}(x,y,z) - \sqrt{2}\mathcal{U}_{02}(x,y,z)). \tag{11}$$

For the sake of compactness and simplicity, we first consider a tilt of the beam occurring at the beam waist location, which we make coincident with the origin of our coordinate system (i.e., $z_0 = 0$). This allows us to simplify our expression of the initial beam to

$$E = E(x,y,0) = E_0 \mathcal{U}_{00}(x,y,0) e^{-i\Psi(0)} e^{i\omega t} = E_0 \mathcal{U}_{00} e^{i\omega t}. \tag{12}$$

Using the approximation in Eq. (8), we can express this beam, tilted by angle α, as

$$E = E_0 \mathcal{U}_{00} e^{i\omega t} \exp\left(\frac{i2\pi\alpha y}{\lambda}\right) \approx E_0 \mathcal{U}_{00} e^{i\omega t} + i\frac{\alpha}{\Theta_{\text{mod}}}\mathcal{U}_{01} e^{i\omega t}, \tag{13}$$

where Θ_{mod} is the far-field beam divergence angle at the tilt-modulator location.

If we now consider a sinusoidal oscillation in the tilt angle such that $\alpha = m_\alpha \cos(\Omega t)$, as could be generated using an EOBD, we obtain, after expanding the cosine into complex exponentials,

$$E \approx E_0 \mathcal{U}_{00} e^{i\omega t} + iE_0 \mathcal{U}_{01} \frac{m_\alpha}{2\Theta_{\text{mod}}}(e^{i(\omega+\Omega)t} + e^{i(\omega-\Omega)t}). \tag{14}$$

The effect of modulating the tilt of the beam is to produce upper and lower sidebands in the HG_{10} mode, which are in phase with each other when in quadrature phase with respect to the carrier HG_{00} mode. This result can be shown to be general for a tilt of the beam occurring at any z axis location.

B. Alignment-Modulated Beam Interaction with a Fabry–Perot Cavity

In this section, we calculate the alignment signals generated in reflection of a Fabry–Perot cavity for both translation of the input beam optic axis with respect to the cavity optic axis and tilt about the cavity eigenmode waist location for an arbitrary angular modulation frequency Ω. The basic optical setup is shown in Fig. 1.

It is necessary at this point to consider the propagation of the alignment-modulated beam described by Eq. (14) from the point of modulation to the cavity waist. We denote the Gouy phase accumulated between the modulator and the cavity waist as $\Delta\Psi$. The HG_{01} mode field components accumulate twice this Gouy phase, and thus accumulate a phase shift of $\Delta\Psi$ relative to the HG_{00} mode components. The angularly modulated beam propagated to the cavity waist location can now be described by

$$E = E_0 \mathcal{U}_{00} e^{i\omega t} + iE_0 \mathcal{U}_{01} e^{-i\Delta\Psi} \frac{m_\alpha}{2\Theta_{\text{mod}}}(e^{i(\omega+\Omega)t} + e^{i(\omega-\Omega)t}). \tag{15}$$

The generality of the z axis location of the modulator relative to the beam waist location in the modulator region is encoded in this accumulated Gouy phase.

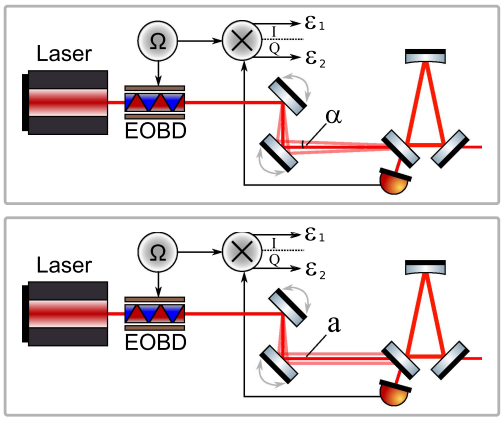

Fig. 1. Basic optical layout considered in this derivation. Jitter modulation sidebands of angular frequency Ω are applied at the EOBD. The signal from the photodetector in reflection of the cavity is demodulated at Ω, in both I and Q phase. Small misalignments of the input beam axis with respect to the cavity axis are applied in tilt (α in the upper panel) and translation (a in the lower panel).

Upon application of a misalignment angle α between the input beam axis and the cavity optical axis at the cavity waist location, the input beam at the cavity waist location may be described in the cavity basis as having an additional transverse phase term,

$$E = E_0\mathcal{U}_{00}e^{i\omega t}\exp\left(\frac{i2\pi\alpha y}{\lambda}\right) + iE_0\mathcal{U}_{01}e^{-i\Delta\Psi}\frac{m_\alpha}{2\Theta_{mod}}(e^{i(\omega+\Omega)t}+e^{i(\omega-\Omega)t})\exp\left(\frac{i2\pi\alpha y}{\lambda}\right). \quad (16)$$

Using the approximations in Eqs. (8) and (9) gives

$$E = E_0\mathcal{U}_{00}e^{i\omega t} + iE_0\mathcal{U}_{01}\frac{\alpha}{\Theta_{cav}}e^{i\omega t} + iE_0\mathcal{U}_{01}e^{-i\Delta\Psi}\frac{m_\alpha}{2\Theta_{mod}}(e^{i(\omega+\Omega)t}+e^{i(\omega-\Omega)t}) - E_0\left(\frac{1}{2}\mathcal{U}_{00}+\frac{1}{\sqrt{2}}\mathcal{U}_{02}\right)e^{-i\Delta\Psi}\frac{\alpha m_\alpha}{\Theta_{cav}\Theta_{mod}}(e^{i(\omega+\Omega)t}+e^{i(\omega-\Omega)t}), \quad (17)$$

where Θ_{cav} is the far-field divergence angle of the cavity eigenmode.

With the aim of detecting an alignment error signal in reflection from the cavity, we must consider the reflected field from the cavity E_{refl}. In reflection from the cavity, each term in Eq. (17) is multiplied by the cavity complex reflectance function $F(\omega, n)$, where n is the horizontal mode index. The complex reflectance is given by

$$F(\omega, n) = r_1 - \frac{r_2t_1^2\exp(-i(D\frac{\omega}{c}+n\Psi_{rt}))}{1-r_1r_2\exp(-i(D\frac{\omega}{c}+n\Psi_{rt}))}, \quad (18)$$

where r_1, t_1, r_2, and t_2 are the amplitude reflectivities and transmissivities of the front and back mirrors, respectively; D is the exact round-trip length of the cavity; and Ψ_{rt} is the Gouy phase accumulated on one round-trip path inside the cavity.

The photocurrent produced by a photodetector in reflection from the cavity is given by

$$I_{PD} = \int_{-\infty}^{\infty}\int_{-\infty}^{\infty}E_{refl}E_{refl}^*dxdy. \quad (19)$$

E_{refl} and E_{refl}^* have 8 terms each, so there are 64 terms to evaluate in the product $E_{refl}E_{refl}^*$. However, we know that many of these terms do not contribute to the photodetector signal after demodulation at the RF modulation frequency Ω and low-pass filtering, and many terms also disappear due to the orthogonality of the higher-order HG mode functions across the photodetector surface (assuming a small beam size relative to the photodetector surface area).

We can compute the integral easily by recognizing that the only dependencies on x and y are contained in the HG spatial functions $\mathcal{U}_{nm}$. We can also use the result arising from the normalization of the HG spatial functions,

$$\int_{-\infty}^{\infty}\int_{-\infty}^{\infty}|\mathcal{U}_{nm}|^2dxdy = 1. \quad (20)$$

The photocurrent is then

$$I_{PD}^{\Omega} = E_0^2\frac{\alpha m_\alpha}{2\Theta_{cav}\Theta_{mod}}(Ae^{-i\Omega t}+A^*e^{i\Omega t}), \quad (21)$$

where A is the complex coefficient

$$A = e^{-i\Delta\Psi}[F(\omega,1)^*F(\omega-\Omega,1) - F(\omega,0)^*F(\omega-\Omega,0)] + e^{i\Delta\Psi}[F(\omega,1)F(\omega+\Omega,1)^* - F(\omega,0)F(\omega+\Omega,0)^*], \quad (22)$$

and we recognize that the complex coefficient associated with the $e^{i\Omega t}$ term is the complex conjugate of that associated with the $e^{-i\Omega t}$ term.

Equation (21) can then be rewritten in terms of the real and imaginary parts of A as

$$I_{PD}^{\Omega} = E_0^2\frac{\alpha}{\Theta_{cav}}\frac{m_\alpha}{\Theta_{mod}}[\Re\{A\}\cos(\Omega t) + \Im\{A\}\sin(\Omega t)]. \quad (23)$$

We will return to this expression shortly, but first we are interested in calculating the equivalent photocurrent produced for an angularly modulated input beam with an optical axis that is *translated* with respect to the cavity optic axis. Using the approximations in Eqs. (10) and (11), we can write the input beam electric field (with angular modulation sidebands) at the cavity waist location for the case where the input beam axis is translated by a with respect to the cavity axis:

$$E = E_0\mathcal{U}_{00}e^{i\omega t} - E_0\mathcal{U}_{01}\frac{a}{w_{0cav}}e^{i\omega t} + iE_0\mathcal{U}_{01}e^{-i\Delta\Psi}\frac{m_\alpha}{2\Theta_{mod}}(e^{i(\omega+\Omega)t}+e^{i(\omega-\Omega)t}) + iE_0\left(\frac{1}{2}\mathcal{U}_{00}-\frac{1}{\sqrt{2}}\mathcal{U}_{02}\right)e^{-i\Delta\Psi}\frac{\alpha m_\alpha}{\Theta_{cav}\Theta_{mod}}(e^{i(\omega+\Omega)t}+e^{i(\omega-\Omega)t}), \quad (24)$$

where w_{0cav} is the cavity waist size. An analysis similar to that performed for the tilted beam yields the following expression

for the photocurrent produced by a photodetector in reflection of the cavity:

$$I_{PD}^{\Omega} = E_0^2 \frac{a m_\alpha}{2 w_{0\mathrm{cav}} \Theta_{\mathrm{mod}}} \mathrm{i}(B e^{-\mathrm{i}\Omega t} - B^* e^{\mathrm{i}\Omega t}), \quad (25)$$

where B is the complex coefficient

$$B = e^{-\mathrm{i}\Delta\Psi}[F(\omega,0)^* F(\omega-\Omega,0) - F(\omega,1)^* F(\omega-\Omega,1)] + e^{\mathrm{i}\Delta\Psi}[F(\omega,1)F(\omega+\Omega,1)^* - F(\omega,0)F(\omega+\Omega,0)^*]. \quad (26)$$

Equation (25) can be expressed in terms of the real and imaginary parts of B as

$$I_{PD}^{\Omega} = E_0^2 \frac{a}{w_{0\mathrm{cav}}} \frac{m_\alpha}{\Theta_{\mathrm{mod}}} [\Re\{B\} \sin(\Omega t) - \Im\{B\} \cos(\Omega t)]. \quad (27)$$

The photocurrent signals shown in Eqs. (23) and (27) can simply be summed to get the total signal from both misalignment degrees of freedom:

$$I_{PD}^{\Omega\alpha a} = E_0^2 \frac{m_\alpha}{\Theta_{\mathrm{mod}}} \left[\left(\frac{\alpha}{\Theta_{\mathrm{cav}}} \Re\{A\} - \frac{a}{w_{0\mathrm{cav}}} \Im\{B\} \right) \cos(\Omega t) + \left(\frac{a}{w_{0\mathrm{cav}}} \Re\{B\} + \frac{\alpha}{\Theta_{\mathrm{cav}}} \Im\{A\} \right) \sin(\Omega t) \right]. \quad (28)$$

C. Demodulation of the Photodetector Signal

To this point we have only retained terms in the photocurrent produced at a photodiode in reflection from the cavity that will remain after demodulation with the original modulation frequency Ω and low-pass filtering. However, we have yet not performed the mathematical operation equivalent to the demodulation stage itself. This step can be described by taking the product of the photocurrent signal (which we may assume is converted to a voltage signal by an appropriate trans-impedance stage with a gain of 1 V/W) with the initial modulation signal, commonly known as the local oscillator,

$$V_{PD}^{\Omega\mathrm{demod}} = I_{PD}^{\Omega} \times \cos(\Omega t + \phi), \quad (29)$$

where ϕ is an additional phase offset applied to the local oscillator. Using $\phi = 0$, a condition often known as *in-phase* or *I-phase* demodulation, we obtain the following expression for the alignment error signal after a low-pass filter removes signal components at 2Ω:

$$V_{PDLPF}^{\Omega\mathrm{Idemod}} = E_0^2 \frac{m_\alpha}{2\Theta_{\mathrm{mod}}} \left(\frac{\alpha}{\Theta_{\mathrm{cav}}} \Re\{A\} - \frac{a}{w_{0\mathrm{cav}}} \Im\{B\} \right). \quad (30)$$

Demodulation with a phase $\phi = \frac{\pi}{2}$, known as Q-phase demodulation, gives the result

$$V_{PDLPF}^{\Omega\mathrm{Qdemod}} = E_0^2 \frac{m_\alpha}{2\Theta_{\mathrm{mod}}} \left(\frac{a}{w_{0\mathrm{cav}}} \Re\{B\} + \frac{\alpha}{\Theta_{\mathrm{cav}}} \Im\{A\} \right). \quad (31)$$

D. Analysis of Error Signals

A qualitative understanding of the way this scheme works can be obtained by considering the various beats that contribute to the signal on the reflection photodiode, and evaluation of the I- and Q-phase signals from Eqs. (30) and (31) for some simple cases. Considering the terms in A and B, there are some simplifications that can be made provided we assume that the cavity length is controlled to be on resonance for the carrier light, and that the total accumulated Gouy phase between the EOBD and the cavity is equal to 2π.

In this case, $F(\omega,0) = F(\omega,0)^*$, since the reflection coefficient is totally real for a resonant field component. In addition to this, we also know that $F(\omega+\Omega,0) = F(\omega-\Omega,0)^*$ and thus $F(\omega-\Omega,0) = F(\omega+\Omega,0)^*$ for fundamental mode sideband field components which are symmetric about the carrier. The assumption of an accumulated Gouy phase of 2π allows us to make the simplification that $e^{-\mathrm{i}\Delta\Psi} = e^{\mathrm{i}\Delta\Psi} = 1$. The effect of having $\Psi \neq \mathrm{n}2\pi$ is to rotate the tilt and translation signal components in the IQ basis, with no effect on the orthogonality property of these signals. Choosing $\Psi = 2\pi$ here just makes the analytical results more intuitively understandable. These simplifications modify the expressions for A and B to

$$A = F(\omega,1)^* F(\omega-\Omega,1) + F(\omega,1)F(\omega+\Omega,1)^* - 2F(\omega,0)F(\omega+\Omega,0)^* \quad (32)$$

$$B = F(\omega,1)F(\omega+\Omega,1)^* - F(\omega,1)^* F(\omega-\Omega,1). \quad (33)$$

Let us next check some simple cases to determine the error signals obtained.

1. Error Signals in the Case of No Cavity

In the case of no cavity at all, we can set all reflectivity coefficients to 0. Clearly in this case, no error signal is derived for either degree of freedom, as expected. If we consider a single mirror with a reflectivity of 1, all reflectivity coefficients are 1, A and B both become zero, and again no error signal is derived, as expected. This analysis proves that alignment signals generated in this way are not simply generated due to spot position change on the photodetector.

2. Error Signals for High-Finesse Impedance Matched Cavity, with Non-Resonant Jitter Sidebands

In the case where the cavity is impedance matched, the reflectivity coefficient for all resonant components drops to zero. For a cavity maintained on resonance for the fundamental mode carrier, the coefficients A and B therefore become

$$A = F(\omega,1)^* F(\omega-\Omega,1) + F(\omega,1)F(\omega+\Omega,1)^*, \quad (34)$$

$$B = F(\omega,1)F(\omega+\Omega,1)^* - F(\omega,1)^* F(\omega-\Omega,1). \quad (35)$$

If we then assume the cavity to have high finesse and to be geometrically stable (such that the carrier frequency HG_{01} mode is not co-resonant with the HG_{00} mode), and that all sideband field components are far away from resonance, we can assume that the reflection coefficients $F(\omega,1)$ and $F(\omega \pm \Omega,1)$ are completely real and also equal to some generic anti-resonant amplitude reflectivity $r \approx 1$. We are therefore left with $A = 2r^2$ and $B = 0$; therefore, for the I- and Q-phase demodulated error signals,

$$V_{PDLPF}^{\Omega\mathrm{Idemod}} \approx E_0^2 \frac{m_\alpha}{\Theta_{\mathrm{mod}}} \frac{\alpha}{\Theta_{\mathrm{cav}}} r^2, \quad (36)$$

$$V_{PDLPF}^{\Omega\mathrm{Qdemod}} \approx 0. \quad (37)$$

Thus it can be seen that we have a linear error signal for the tilt of the input beam axis with respect to cavity axis about the cavity waist in the I-phase signal, and no signal at all in the Q-phase demodulated signal. This is exactly the typical situation for *dither*

alignment sensing. With dither alignment sensing, only the degree of freedom that is dithered is sensed. In this case with 2π accumulated Gouy phase between EOBD and cavity waist, the dithered degree of freedom is the tilt degree of freedom, and thus the tilt degree of freedom is the only one sensed.

3. Error Signals for High-Finesse Impedance Matched Cavity with One Resonant Jitter Sideband

If we further stipulate that the modulation frequency is set equal to the higher-order mode difference frequency of the cavity, then the upper alignment modulation sideband becomes resonant and its reflectivity coefficient also drops to zero, giving

$$A = F(\omega, 1)^* F(\omega - \Omega, 1), \tag{38}$$

$$B = -A = -F(\omega, 1)^* F(\omega - \Omega, 1). \tag{39}$$

We then apply the same assumptions of high-finesse and geometric stability to obtain for the I- and Q-phase demodulated error signals:

$$V_{PDLPF}^{\Omega\text{Idemod}} \approx E_0^2 \frac{m_\alpha}{2\Theta_{\text{mod}}} \frac{\alpha}{\Theta_{\text{cav}}} r^2, \tag{40}$$

$$V_{PDLPF}^{\Omega\text{Qdemod}} \approx -E_0^2 \frac{m_\alpha}{2\Theta_{\text{mod}}} \frac{a}{w_{0cav}} r^2. \tag{41}$$

Here it is clear that the I-phase signal is linear in angular misalignment α and insensitive to the translational misalignment a, whereas conversely the Q-phase signal is linear in translational misalignment but insensitive to angular misalignment. Thus we show that the scheme allows the recovery of well-separated error signals for both alignment degrees of freedom from just one single element photodetector in reflection of the cavity, as long as the modulation frequency is made equal to the higher-order mode difference frequency of the cavity.

The simple qualitative argument as to why the matching of the modulation frequency to the higher-order mode difference frequency allows for reconstruction of well-separated alignment signals in the orthogonal demodulation phases rests on the breaking of the symmetry between upper and lower angular modulation sidebands. When one sideband is resonant in the cavity, the symmetry between these sidebands is broken, and so misalignment in either degree of freedom produces amplitude modulation, which is detectable by a photodiode. With symmetric sidebands, on the other hand, the non-dithered degree of freedom produces only undetectable phase modulation. With sideband asymmetry, the Q-phase signal does not vanish, but carries instead information about the non-dithered alignment degree of freedom. This fact is effectively the reason why the Anderson alignment sensing scheme can recover well-separated signals with a single *quadrant* photodetector [6]; our approach is the same, but we use only a single-element photodetector.

4. Error Signals for High-Finesse Over-Coupled Cavity with One Resonant Jitter Sideband

Here we demonstrate that the scheme also provides useful error signals in the case of a completely over-coupled cavity, where the cavity output mirror has a reflectivity of 1. In this case, under the same assumptions as before (high-finesse, geometrically stable, angular modulation frequency equal to higher-order mode difference frequency) all reflectivity coefficients are real, and either equal to 1 for non-resonant field components, or -1 for resonant field components. This gives us $A = 2$ and $B = -2$, and accordingly for the I- and Q-phase demodulated error signals,

$$V_{PDLPF}^{\Omega\text{Idemod}} \approx E_0^2 \frac{m_\alpha}{\Theta_{\text{mod}}} \frac{\alpha}{\Theta_{\text{cav}}}, \tag{42}$$

$$V_{PDLPF}^{\Omega\text{Qdemod}} \approx -E_0^2 \frac{m_\alpha}{\Theta_{\text{mod}}} \frac{a}{w_{0cav}}. \tag{43}$$

It is worth noting that in the totally over-coupled case, dither alignment sensing is a poor method for sensing misalignment, as can be seen when the A coefficient is evaluated for $F(\omega, 0) = -1$ and all other field components have a reflectivity from the cavity of 1. In this case, A vanishes, and no error signal can be obtained in reflection from the cavity, even for the degree of freedom which is dithered.

5. Comparison with Finesse Simulation

In this section, we numerically evaluate the response of I- and Q-phase error signals to translation and tilt of the input beam with respect to the cavity eigenmode. We simulate a cavity with a free spectral range of 135 MHz, a finesse of 59, and a higher-order mode spacing of 14.7 MHz. The parameters were based on those of the cavity used in the experiments described in Section 3, listed as Cavity 1 in Table 1.

In order to verify the analytical calculations, the same optical setup was simulated using the open-source frequency-domain interferometer simulation tool FINESSE [7]. This software numerically evaluates couplings between HG modes caused by misalignments and mode mismatches in interferometers using analytical expressions derived by Bayer-Helms in Ref. [11].

Figure 2 shows the results from the FINESSE simulation overlaid with the analytically derived error signals for the cavity described previously. The results are practically identical, showing a good agreement between the analytically derived error signals and the numerical simulation. This figure also demonstrates the usefulness of this alignment sensing scheme, because it can be clearly seen that when the EOBD modulation frequency is equal to the cavity higher-order mode difference frequency, the I-phase signal responds to translation of the input beam only, and the Q-phase signal responds to tilt of the input beam only. Therefore, well-separated alignment signals can be generated with just one single-element photodetector in reflection of the cavity.

Table 1. Parameters of the Cavities Used in the Experimental Demonstrations, and also in the Numerical Calculations in Section 2.D.5

Parameter	Cavity 1	Cavity 2	Cavity 3	Units
Round-trip length	2.2	0.42	1.4	m
End mirror Rc	9.8	1	2	m
Free spectral range	135	714	214	MHz
Round-trip Gouy phase	39	55	73	deg
$\delta\nu_{\text{HOM}}$	14.7	108	43.26	MHz
Finesse	59	350	1030	

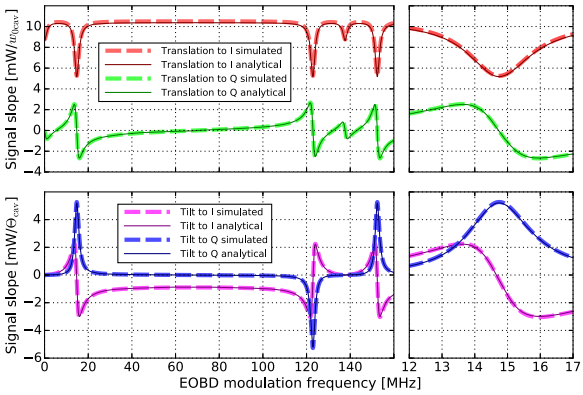

Fig. 2. Response of the demodulated photodetector signal to translation (upper panels) and tilt (lower panels) of the input beam for the Fabry–Perot cavity described in Table 1, calculated both with the analytical results from Section C and FINESSE. The lowest frequency peak corresponds to resonance of the upper jitter sideband, whereas the second peak corresponds to the resonance of the lower jitter sideband. The third peak corresponds to the resonance of HG_{00} mode sideband field components, and the fourth peak is the resonance of the upper jitter sideband at the next cavity FSR. A zoom-in around the upper jitter sideband resonance is shown in the right hand panels. When one of the jitter sidebands is resonant, the response of the Q-phase signal to translations goes to zero, while that of the I-phase signal remains finite, and vice versa for tilt.

3. EXPERIMENTAL DEMONSTRATION

A. Design of the Electro-Optic Beam Deflector

The alignment sensing method under investigation is reliant upon the use of a high-frequency (>1 MHz) alignment actuator in order to produce HG_{10} or HG_{01} mode sidebands that will co-resonate in an optical cavity with the carrier light. Mechanical alignment actuators such as Piezo transducer (PZT) mounted mirrors or galvanometer assemblies are typically limited to 1 kHz or below in bandwidth, making them unsuitable for this application. EOBDs, on the other hand, can in principle operate up to very high frequencies. Our experiments made use of a custom-built EOBD, based on either a rubidium titanyl phosphate (RTP) crystal or lithium niobate ($LiNbO_3$) crystal sandwiched between two specially designed copper electrodes. The EOBD design is based on the design reported in Ref. [10], although we use crystals for the electro-optic material rather than polymers due to the higher optical quality and power handling ability of crystals. The electrode arrangement allows for the generation of electro-optic prisms inside the crystal, causing a deflection of a beam crossing the boundaries between high and low index regions. Further details on the EOBD design and operation are reported in [12].

B. Alignment Error Signals for a Fabry–Perot Cavity

The experimental layout for the initial demonstration is shown in Fig. 3. The beam from a 1064 nm Nd:YAG laser was passed through an electro-optic phase modulator (EOM) and a $LiNbO_3$ EOBD. The EOM was driven with a fixed 26.717 MHz sine wave to produce phase modulation sidebands which are used to generate the laser frequency error signal and

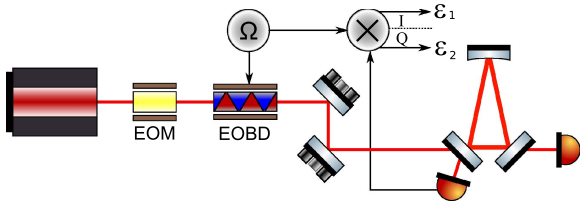

Fig. 3. Experimental layout for the demonstration of the alignment sensing scheme on a single optical cavity. A lock-in amplifier provides the RF signal to drive the EOBD, and also demodulates the cavity reflection photodiode in I and Q phase to provide the alignment error signal. A Labview program provides the slow modulation of cavity alignment in tilt and translation sequentially, while also setting the RF modulation frequency and acquiring the demodulated error signals.

lock the laser frequency to the cavity resonance. The EOBD was driven with a tunable frequency sine wave from a Zurich Instruments lock-in amplifier, providing deflection of the beam out of the plane of the table. The EOBD produces alignment modulation sidebands on the carrier light, as described in Section 3.A.

The modulated beam was then passed to a triangular optical cavity via two PZT-actuated steering mirrors. The cavity parameters are listed under Cavity 1 in Table 1. The reflected light from the cavity was detected with a single-element photodetector. The signal from this detector was split, with one copy being demodulated at the EOM modulation frequency to provide the PDH length/frequency error signal. This signal was fed back to the laser in order to keep the cavity on resonance. The other copy of the reflected light signal was demodulated by the lock-in amplifier at the EOBD modulation frequency, and the I- and Q-phase demodulated signals were acquired in a Labview program via an analog to digital converter (ADC). The two PZT-actuated mirrors were driven sinusoidally at 23 Hz with the same Labview program via a digital to analog converter (DAC). The amplitude and phase of the PZT drive signals were chosen so as to create either a pure tilt of the beam at the cavity waist, or a pure translation of the beam with respect to the cavity axis. Both tilt and translation degrees were driven in the pitch axis (out of the plane of the cavity).

The alignment error signals for translation and tilt are shown in Fig. 4, for the case where the EOBD modulation frequency was 14.7 MHz, close or equal to the higher-order mode frequency spacing $\delta\nu_{\mathrm{HOM}}$ of the triangular cavity. The demodulation phase of the lock-in amplifier was adjusted in order to minimize the appearance of the translation signal in the Q-phase output. The same demodulation phase was used when observing the response to the tilt of the beam. The translation signal appears almost exclusively in the I-phase output, while the tilt signal appears almost exclusively in the Q-phase output. In contrast, for modulation frequencies far away from the cavity $\delta\nu_{\mathrm{HOM}}$, it was observed that only one combination of the two alignment degrees of freedom could be sensed, as shown in Fig. 5.

The undemodulated signal from the cavity transmitted light is also shown in the plots, with the mean value subtracted in order to preserve a suitable y-axis scale. The transmitted light signal predominantly shows the second harmonic of the PZT

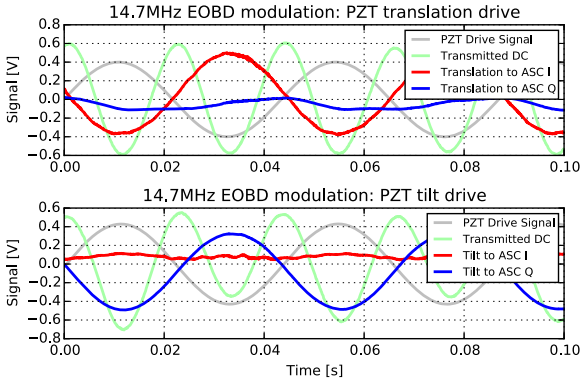

Fig. 4. Time series of I and Q demodulated error signals while driving the translation (upper plot) and tilt (lower plot) pitch degrees of freedom, with angular modulation frequency equal to the cavity $\delta\nu_{\mathrm{HOM}}$. The translation signal appears in the I output, while the tilt signal appears in the Q output.

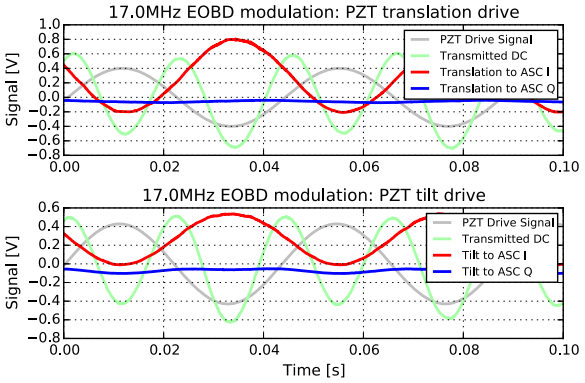

Fig. 5. Time series of I and Q demodulated error signals while driving the translation (upper plot) and tilt (lower plot) pitch degrees of freedom, with angular modulation frequency far from the cavity $\delta\nu_{\mathrm{HOM}}$. The translation and tilt signals appear in the I output, while the Q output is unresponsive to either alignment degree of freedom.

drive frequency, indicating by virtue of the quadratic coupling from input misalignment to transmitted light intensity that the mean alignment was good. This also demonstrates that the I and Q error signals shown are not simply the result of a fixed RF amplitude modulation on the beam being modulated at the PZT drive frequency because of a large alignment offset.

These measurements can also be presented as a *sensing matrix*, by determining the amplitudes of the I- and Q-phase responses to tilt and translation drive. A diagonal sensing matrix is ideal for sensing the two considered alignment degrees of freedom independently. Table 2 shows the sensing matrices calculated for the two measurements shown in Figs. 4 and 5, normalized in each case by the translation drive to I-phase signal amplitude. The sensing matrix obtained for the 14.7 MHz modulation frequency (where $\Omega = \delta\nu_{\mathrm{HOM}}$) is close to diagonal, whereas the matrix generated for the 17 MHz modulation frequency (where $\Omega > \delta\nu_{\mathrm{HOM}}$) is far from diagonal.

Table 2. Alignment-Sensing Matrices Generated for Cavity 1 at Two Different Alignment Modulation Frequencies

	14.7 MHz	
	Translation	Tilt
I	1	−0.03
Q	0.06	−0.93
	17.0 MHz	
	Translation	Tilt
I	1	0.55
Q	−0.04	0.02

These results agree with the prediction made in Section 2.D.2 that unless the alignment modulation frequency matches the cavity $\delta\nu_{\mathrm{HOM}}$, the result is effectively equivalent to dither alignment sensing, where only the dithered degree of freedom is sensed. In this experiment, the dithered degree of freedom was some combination of tilt and translation, or in other words, $\Delta\Psi \neq \frac{n\pi}{2}$.

C. Alignment Error Signals for a Downstream Cavity

The ability to generate a diagonal sensing matrix with the technique demonstrated in Section 2.B relies on the resonance of one of the higher-order mode sidebands in the cavity breaking the symmetry between upper and lower sidebands. The beam transmitted through the first cavity will be composed of the fundamental mode carrier light and the resonant higher-order mode sideband. The non-resonant higher-order mode sideband will be reflected from the first cavity (it is this non-resonant sideband that provides the alignment signals for the first cavity). The beam transmitted through the first cavity therefore already exhibits a sideband asymmetry, which will allow the generation of a diagonal alignment sensing matrix for a second downstream cavity *without* the requirement that one jitter sideband is resonant in the second cavity.

Figure 6 shows the experimental layout for demonstrating the alignment sensing of a second downstream cavity. The second cavity is a copy of the Advanced LIGO pre-stabilized laser diagnostic breadboard cavity [13]. Its parameters are listed under Cavity 2 in Table 1. A second EOM was placed in between the two cavities in order to produce another set of phase modulation sidebands at 33 MHz. A photodiode in reflection of the second cavity was demodulated with the 33 MHz signal to generate a PDH length error signal for the second cavity. This error signal was fed back to a PZT attached to the end mirror of the second cavity to keep the cavity locked to the laser frequency.

A copy of the same photodiode signal was also demodulated with the 14.7 MHz frequency which was driving the EOBD. The I and Q demodulated outputs were recorded while the second set of PZT steering mirrors were used to slowly modulate the alignment into the second cavity at 21 Hz, in both tilt and translation degrees of freedom in turn. The recorded time series are shown in Fig. 7. The I-phase demodulated signal responds mainly to the tilt degree of freedom, while the Q-phase demodulated signal responds mainly to the translation degree of freedom. These results are summarized in the alignment sensing matrix shown in Table 3 (this time with the elements

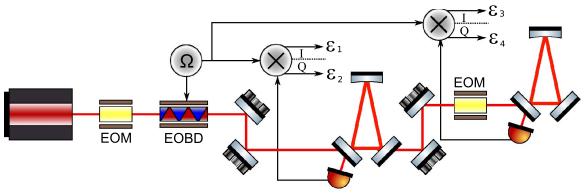

Fig. 6. Experimental layout for measuring alignment signals for a downstream cavity with the RF jitter method. The laser was locked to the first optical cavity, and the EOBD modulation frequency was matched to the higher-order mode spacing of the first cavity. The second cavity was locked to the laser, and the alignment error signals were produced by demodulating the reflected light at the EOBD drive frequency.

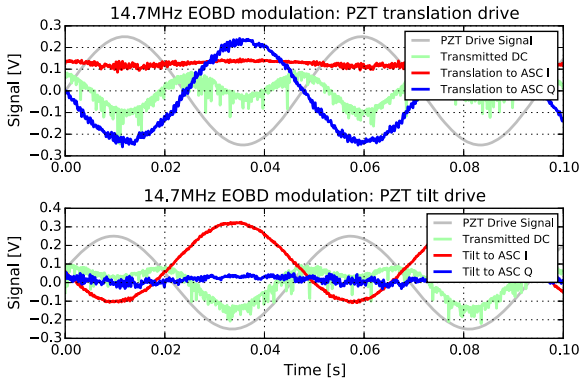

Fig. 7. Time series of I and Q demodulated error signals for Cavity 2, downstream of Cavity 1, while driving the translation (upper plot) and tilt (lower plot) pitch degrees of freedom. The angular modulation frequency applied to the EOBD was 14.7 MHz, equal to the Cavity 1 $\delta\nu_{\mathrm{HOM}}$. The tilt signal appears in the I output, while the translation signal appears in the Q output.

Table 3. Alignment-Sensing Matrix Generated for Cavity 2, Downstream of Cavity 1, for a Modulation Frequency Equal to the Higher-Order Mode Difference Frequency of Cavity 1

	14.7 MHz	
	Translation	**Tilt**
I	0.06	0.91
Q	1	0.07

normalized by the translation to Q-phase signal), where it can be seen that the sensing matrix is close to diagonal. The higher finesse of the second cavity, combined with a non-optimized PDH lock, resulted in a noisier transmitted light signal for this cavity.

This aspect of the alignment sensing technique in particular could have important applications in gravitational wave detectors like Advanced LIGO. A possible implementation of this scheme would involve EOBDs placed before the input mode cleaner (IMC), modulated at f_{pit} and f_{yaw}; the higher-order mode difference frequencies for pitch and yaw axes of the

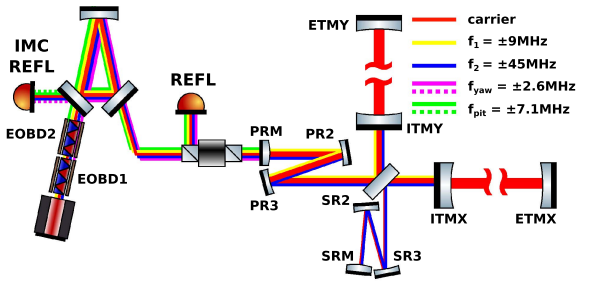

Fig. 8. Illustration for how the alignment sensing scheme described in this paper might be applied to Advanced LIGO. Different colored beams indicate different frequency components of the laser field. For the jitter sidebands, which have an asymmetric interaction with the IMC, the lower sidebands are shown by the dashed lines.

IMC, respectively. The signals from the IMC reflected light, demodulated at f_{pit} and f_{yaw}, could provide alignment signals for the IMC. The jitter sidebands that are transmitted through the IMC could also be used to produce useful alignment signals for the core interferometer. Detecting the beats between the IMC transmitted jitter sidebands and the carrier, as well as beats between the jitter sidebands and the phase modulation sidebands already present in the main interferometer [14], could provide useful alignment signals for the optical cavities that make up the Advanced LIGO core interferometers. Figure 8 shows a sketch of the relevant field components in an Advanced LIGO interferometer as an illustration of how this scheme could be implemented.

D. Modulation Frequency Dependence of Alignment Error Signals

A series of similar measurements were performed over a range of EOBD modulation frequencies, in order to determine the frequency dependence of the alignment sensing matrices that can be generated with this method and compare with the theoretical expectation. Preliminary measurements, made with the same cavity used for the measurements shown in Figs. 4 and 5 (Cavity 1 in Table 1), showed broadly the expected behavior, but resonances of the EOBD itself caused sharp features in the measured frequency dependence of the alignment sensing matrix. A third cavity (listed as Cavity 3 in Table 1) was therefore built with a higher finesse, constraining the interesting part of the frequency dependence to a smaller frequency band between EOBD resonances. An RTP EOBD was also used for this experiment, under the expectation that the smaller piezoelectric coefficient of RTP compared to $LiNbO_3$ would mitigate any mechanical resonance effects. The results of the measurement from the third cavity are shown in Fig. 9, along with the outputs from an analytically derived model of the same optical setup.

The data shown in Fig. 9 were extracted from the time series data recorded for each EOBD modulation frequency (similar to those shown in Figs. 4, 5, and 7) in the following way. First, a sine function at the PZT drive frequency was fit to the recorded PZT drive signal, in order to determine the appropriate phase for analyzing the lock-in I and Q outputs (alignment error signals). Then sine functions at the PZT drive frequency were fit to the recorded I- and Q-phase signals from the lock-in amplifier,

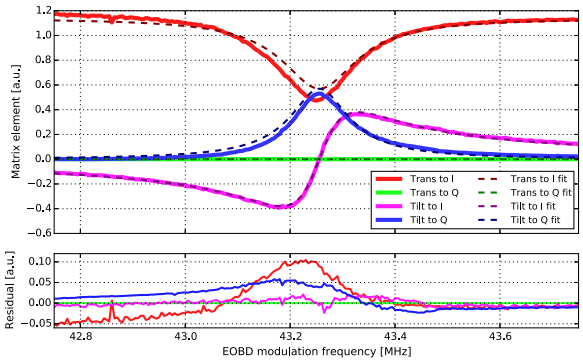

Fig. 9. Measured frequency dependence of the alignment sensing matrix generated with the alignment sensing scheme. The measured data is overlaid with the results from a fit of the analytical model described in Section 2 to the data. The lower trace shows the residuals between the fitted analytical model and the data.

allowing the voltage offset and amplitude to be adjusted by the fit, but maintaining the fixed phase determined from fitting the drive signal. Following this procedure for one EOBD modulation frequency enables the construction of a raw sensing matrix, similar to those shown in Tables 2 and 3, from the fitted amplitudes of I and Q outputs for translation and tilt.

When sweeping the EOBD modulation frequency, the lock-in demodulation phase could not be adjusted by hand to minimize the translation to Q-phase signal, because this optimal demodulation phase is frequency-dependent on account of the cavity interaction and other delays in the optical and RF electrical paths. Instead, the equivalent procedure was performed in software on the raw sensing matrix, by creating complex numbers of the form $x_{\mathrm{DOF}} = I_{\mathrm{DOF}} + \mathrm{i}Q_{\mathrm{DOF}}$ for both translation and tilt. The argument of this number was determined for translation, and then both the translation and tilt complex numbers were rotated in the complex plane by this angle, resulting in the elimination of the imaginary part of the translation complex number. The sensing matrix can then be recomposed from the real and imaginary parts of the rotated complex numbers.

The phase-rotated sensing matrices are plotted as a function of EOBD modulation frequency in Fig. 9. The blue and red traces represent the on-diagonal elements of the alignment sensing matrix, while the green and pink traces represent the off-diagonal elements. The sensing matrix is most diagonal at an EOBD modulation frequency of around 43.25 MHz; the higher-order mode difference frequency of the cavity. As the modulation frequency is varied away from this value, the off-diagonal elements increase in size relative to the on-diagonal elements. Far away from the higher-order mode difference frequency of the cavity, the error signals obtained are similar to those that would be obtained with a simple dither sensing technique, where only the combination of alignment degrees of freedom which are modulated can be sensed.

Figure 9 also shows the results of fitting the analytically derived frequency-dependent error signal response to the measured data. The free parameters in the fit were the accumulated Gouy phase between the EOBD and the cavity waist, the radius of curvature of the cavity end mirror, an overall y-axis scaling factor and the reflectivities of the input and output couplers of the cavity (assumed to be equal for an impedance matched cavity). The fitted end mirror radius of curvature and measured cavity length were used to calculate the value of $\delta\nu_{\mathrm{HOM}}$ shown in Table 1, and the fitted mirror reflectivities were used to calculate the cavity finesse. The fitted accumulated Gouy phase $\Delta\Psi$ was 89.9°; very close to the experimentally aimed-for 90°.

The fitting residuals shown in the lower plot of Fig. 9 are small, indicating that the analytical model provides a good description of the measured frequency dependence of the alignment sensing matrix. Possible sources of the remaining discrepancy between the data and the model are imperfect diagonalization of the PZT drive matrix, and unequal drive amplitudes of the two degrees of freedom in natural beam units.

The frequency dependence of the I-phase output response to tilt misalignment indicates that such a signal could potentially be used as an error signal to use for matching the EOBD modulation frequency to the cavity higher-order mode spacing. In the event of any thermal lensing in the cavity (or other sources of variation in the cavity geometry), this approach would prove useful both as a cavity geometry probe and as a means of maintaining optimal diagonalization of the alignment sensing matrix. A low-bandwidth EOBD modulation frequency error signal could be derived by performing a slow dither of the tilt degree of freedom and double demodulating the reflected light signal; once at the EOBD drive frequency, and then demodulating the I-phase output of the first demodulation again at the slower tilt dither frequency.

4. CONCLUSIONS

In this paper, we have described a new method for sensing misalignments between a laser beam and an optical cavity. This method does not rely on the use of split photodetectors. We have derived the alignment signals analytically, and demonstrated a good agreement with numerical simulations performed with FINESSE. We have performed an experimental demonstration, showing that well-separated cavity alignment signals can be generated for two degrees of freedom in one axis by modulating the input beam alignment at the higher-order mode difference frequency of the cavity, and performing IQ demodulation of the reflected light signal at the modulation frequency. The modulation-frequency dependence of these alignment signals was measured, and shown to have a good agreement with the theory. Furthermore, we demonstrated experimentally that well-separated alignment signals could be generated for a second downstream cavity without the requirement that the modulation frequency matches the higher-order mode difference frequency of the second cavity.

There are several potential advantages to an alignment sensing scheme that does not rely on the use of RF split photodetectors. One challenge with RF split detectors is to make the photodiode elements small enough that the capacitance remains low, so that the bandwidth of the detector still allows for RF detection. However, making the elements small typically means that the gap region is larger relative to the beam spot size, leading to a lower effective quantum efficiency. Efforts to reduce the gap region further often have the drawback of increasing electromagnetic

crosstalk between elements. A high bias voltage can be used to increase the bandwidth of larger area photodetector elements, but this brings with it the problem of bias voltage noise. Thus, a compromise is usually reached between bias voltage, gap size, and element area (and correspondingly beam size) in order to reach the bandwidth and noise characteristics required for a specific application. Relying on the use of only single-element RF detectors, the scheme presented in this paper eliminates the need for compromise in many of these areas.

Another challenge with the use of RF split detectors is the centering of the beam on the detector. Mode mismatches and other non-alignment-related beam distortions can couple into the derived alignment signal in the presence of a miscentering of the beam on the split detector [4]. Beam drift over time typically results in the requirement for an additional DC beam-centering loop. In the case of the alignment scheme presented here, however, the only requirement on centering is that the whole beam is incident on the single element photodetector, which is easily achieved by focusing the beam to a small spot size on a relatively large detector. Our scheme makes use of IQ demodulation to generate separate error signals for the two quadratures of misalignment (categorized in this paper as translation and tilt) with just a single photodetector. In the currently favored wavefront sensing scheme, two split photodetectors are required to measure the two degrees of freedom. Furthermore, these two detectors must be separated by 90° Gouy phase, requiring the careful design and implementation of a so-called Gouy phase telescope. The scheme presented in this paper potentially offers a complexity saving in this respect. The shot noise sensitivity of the presented scheme is theoretically identical to that of the traditional wavefront sensing with split detectors. However, it is likely to be easier to make this detection scheme shot-noise-limited, because of the reduced complexity in single element photodetector design.

It should be noted, however, that the work described in this paper demonstrated the alignment sensing scheme on one axis only (out of the cavity plane, a.k.a pitch). Extension to both axes is trivial in principle, but would require the use of a second beam deflector oriented such as to produce in-plane angular modulation (a.k.a. yaw). For cavities consisting of an odd number of mirrors, the resonant frequencies of misalignment modes caused by in-plane misalignment are separated from the out-of-plane misalignment modes by half a free spectral range (FSR), making it easy to find suitable independent modulation frequencies for both axes. In the case of a cavity composed of an even number of mirrors, one could simply separate the modulation frequencies for the two axes by one or more FSRs.

This scheme can be extended to detect a range of other mismatches between laser beams and optical cavities, provided that the mismatch in question can be modulated rapidly by an electro-optic device. Of particular interest would be an electro-optic lens device, which could be used to generate LG_{10} mode sidebands at twice the higher-order mode difference frequency of an optical cavity. A very similar implementation of such a device as that described in this paper for the EOBD would yield useful mode mismatch error signals. Such a scheme could prove very useful in determining and correcting mode mismatches in future gravitational wave detectors, especially in the optical loss-critical era of squeezed light injection [15,16].

Funding. National Science Foundation (NSF) (PHY-1306594, PHY-1505598).

Acknowledgment. The authors thank Daniel Brown and Andreas Freise for their support with the FINESSE modeling reported in this paper.

REFERENCES

1. R. W. P. Drever, J. L. Hall, F. V. Kowalski, J. Hough, G. M. Ford, A. J. Munley, and H. Ward, "Laser phase and frequency stabilization using an optical resonator," Appl. Phys. B **31**, 97–105 (1983).
2. LIGO Scientific Collaboration and Virgo Collaboration, "Observation of gravitational waves from a binary black hole merger," Phys. Rev. Lett. **116**, 061102 (2016).
3. LIGO Scientific Collaboration and Virgo Collaboration, "GW150914: the advanced LIGO detectors in the era of first discoveries," Phys. Rev. Lett. **116**, 131103 (2016).
4. E. Morrison, B. J. Meers, D. I. Robertson, and H. Ward, "Automatic alignment of optical interferometers," Appl. Opt. **33**, 5041–5049 (1994).
5. E. Morrison, D. I. Robertson, H. Ward, and B. J. Meers, "Experimental demonstration of an automatic alignment system for optical interferometers," Appl. Opt. **33**, 5037–5040 (1994).
6. D. Z. Anderson, "Alignment of resonant optical cavities," Appl. Opt. **23**, 2944–2949 (1984).
7. A. Freise, G. Heinzel, H. Lück, R. Schilling, B. Willke, and K. Danzmann, "Frequency-domain interferometer simulation with higher-order spatial modes," Classical Quantum Gravity **21**, S1067–S1074 (2004).
8. F. S. Chen, J. E. Geusic, S. K. Kurtz, J. G. Skinner, and S. H. Wemple, "Light modulation and beam deflection with potassium tantalate-niobate crystals," J. Appl. Phys. **37**, 388–398 (1966).
9. C. S. Tsai and P. Saunier, "Ultrafast guided-light beam deflection/switching and modulation using simulated electro-optic prism structures in $LiNbO_3$ waveguides," Appl. Phys. Lett. **27**, 248–250 (1975).
10. L. Sun, J.-h. Kim, C.-H. Jang, D. An, X. Lu, Q. Zhou, J. M. Taboada, R. T. Chen, J. J. Maki, S. Tang, H. Zhang, W. H. Steier, C. H. Zhang, and L. R. Dalton, "Polymeric waveguide prism-based electro-optic beam deflector," Opt. Eng. **40**, 1217–1222 (2001).
11. F. Bayer-Helms, "Coupling coefficients of an incident wave and the modes of a spherical optical resonator in the case of mismatching and misalignment," Appl. Opt. **23**, 1369–1380 (1984).
12. D. Voss, "Fast alignment control of an optical resonator," Ph.D. dissertation (University of Florida, 2015).
13. P. Kwee, F. Seifert, B. Willke, and K. Danzmann, "Laser beam quality and pointing measurement with an optical resonator," Rev. Sci. Instrum. **78**, 073103 (2007).
14. K. Izumi and D. Sigg, "Advanced LIGO: length sensing and control in a dual recycled interferometric gravitational wave antenna," Classical Quantum Gravity **34**, 015001 (2017).
15. LIGO Scientific Collaboration, "Enhanced sensitivity of the LIGO gravitational wave detector by using squeezed states of light," Nat. Photonics **7**, 613–619 (2013).
16. M. Evans, L. Barsotti, P. Kwee, J. Harms, and H. Miao, "Realistic filter cavities for advanced gravitational wave detectors," Phys. Rev. D **88**, 022002 (2013).